




# Physical-Layer Network Coding Enhanced Visible Light Communications Using RGB LEDs

Jian Xiong, Runxin Zhang, Lu Lu , *Member, IEEE*, Qifu Tyler Sun , *Member, IEEE*, and Keping Long 

**Abstract**—Visible light communications (VLC) is a good candidate technology for the 6th generation (6G) wireless communications. Red, green, and blue (RGB) light-emitting diodes (LEDs) based VLC has become an important research branch due to its low price and high reliability. However, the saturation of photodiode (PD) caused by the ambient background light may seriously degrade the bit error rate (BER) performance of an RGB-VLC system's three spatially uncoupled information streams (i.e., red, green, and blue LEDs can transmit different data packets simultaneously) in practical applications. To mitigate the ambient light interference in point-to-point RGB-VLC systems, we propose, PNC-VLC, a network-coded scheme that uses two LEDs with the same color at the transmitter to transmit two different data streams and we make use of the naturally overlapped signals at the receiver to formulate physical-layer network coding (PNC). The adaptivity of PNC-VLC could effectively improve the BER degradation problem caused by the saturation of PD under the influence of ambient light. We conducted simulations based on the parameters of commercial off-the-shelf (COTS) products to prove the superiority of the PNC-VLC under the influence of four typical illuminants. Simulation results show that the PNC-VLC system can maintain a better and more stable system BER performance under different ambient background light conditions. Remarkably, with 2/3 throughput efficiency, PNC-VLC can bring 133.3% gain to the BER performance when compared with RGB-VLC under the Illuminant A interference model, making it a good option for VLC applications with unpredictable ambient background interferences.

**Index Terms**—Visible light communications, physical-layer network coding, ambient light noise, photodiode saturation.

## I. INTRODUCTION

**V**ISIBLE Light Communication (VLC) has great potential in high-speed wireless connectivity and has attracted a lot of attention in recent years with operation in the unlicensed

optical spectrum [1]. Light fidelity (LiFi) is an extended concept of VLC and has caught the focus of IEEE 802.11 working group for local area networks to form the amendment TG - 802.11bb, aiming to accelerate the development of LiFi mass-market [2]. The hybrid LiFi and WiFi network, which combines the advantages of both networks, has also been studied [3] and the system has been successfully implemented utilizing IEEE 802.11 MIMO capabilities [4].

Among many VLC solutions, a laser diode (LD) or light-emitting diode (LED) is commonly used to generate an optical signal at the transmitter [5]. The avalanche photodiode (APD) and PIN photodiodes are widely used to detect the optical signal at the receiver. These optoelectronic devices are commonly applied in optical communication, such as fiber communication, and each has advantages and disadvantages. Using an LD as the transmitter can easily realize high-speed communication beyond Gbps [6], [7]. However, high cost and harsh operating conditions limit the development of the LD-VLC scheme. In contrast, using LEDs as the transmitter brings low cost and reliability to the VLC system. In addition, adopting different color LEDs can easily multiply the channel capacity, just like wavelength division multiplexing (WDM) [8]. Therefore, the tricolor LED is more able to implement the VLC system. Considering the demand for illumination, it is difficult to establish the same three VLC links with tricolor LEDs due to the extra consideration of correlated color temperature (CCT) and color reproduction index (CRI). They may also not tolerate a worse lighting effect for a high-speed connection.

In photoelectric detectors, the APD is more sensitive to a weak optical signal and has better performance than PIN when the power of an incident optical signal is lower than  $-20$  dBm [9]. In contrast, in a VLC environment, the receiver may suffer from complex ambient light and the received optical power may be far beyond  $-20$  dBm. Therefore, the APD has no advantages over PIN in VLC [10]. In addition, the high responsivity means that it is easier to be saturated in practical use. When saturation occurs, the output current of the PD no longer keeps a linear relationship with the incident optical signal and the output AC signal will gradually diminish until it disappears, which has seldom been studied in previous research [11]. In most VLC scenarios, the line of sight (LoS) channel gain is primarily considered and the non-line of sight (NLoS) optical channel gain is unimportant when existing LoS channel gain [12].

Physical-layer network coding (PNC) can double the throughput of a two-way relay network (TWRN) by turning interference into useful network-coded messages [13], [14]. Compared with

Manuscript received 1 December 2022; revised 12 January 2023; accepted 25 January 2023. Date of publication 30 January 2023; date of current version 13 February 2023. The work of Jian Xiong, Qifu Tyler Sun, and Keping Long was supported in part by the National Natural Science Foundation of China under Grant 62271044. The work of Runxin Zhang and Lu Lu was supported in part by the Key Research Program of the Chinese Academy of Sciences under Grant ZDRW-KT-2019-1-0103. (Corresponding author: Lu Lu.)

Jian Xiong, Qifu Tyler Sun, and Keping Long are with the School of Computer and Communication Engineering, University of Science and Technology Beijing, Beijing, China (e-mail: b20190305@xs.ustb.edu.cn; qfsun@ustb.edu.cn; longkeping@ustb.edu.cn).

Runxin Zhang and Lu Lu are with the Key Laboratory of Space Utilization, Technology and Engineering Center for Space Utilization, Chinese Academy of Sciences, Beijing 100094, China, and also with the University of Chinese Academy of Sciences, Beijing 100049, China (e-mail: zhangrunxin20@mails.u.ac.cn; lulu@csu.ac.cn).

Digital Object Identifier 10.1109/JPHOT.2023.3240438

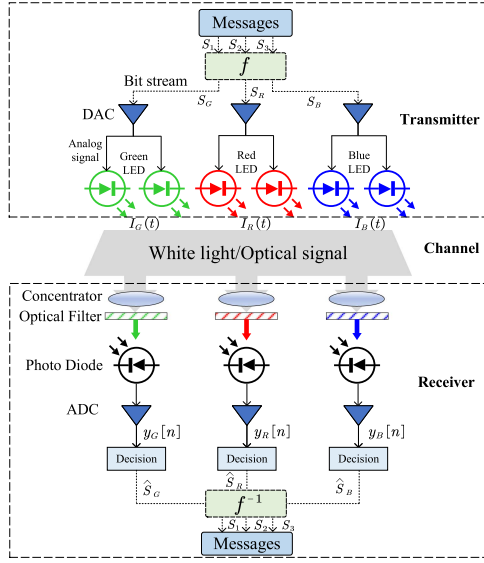


Fig. 1. A traditional VLC system based on RGB LEDs.

the traditional store-and-forward relay scheme, PNC minimizes the time slots needed to exchange information in TWRN, and hence boosts the throughput [15]. Optical PNC (OPNC) was proposed to reduce the link resources needed for network protection by using polarization-multiplexing [16]. OPNC can also boost network efficiency [17], increase system throughput [18], improve spectrum efficiency in passive optical interconnect (POI) networks [19] and reduce the usage of wavelength resources [20]. The application of OPNC in VLC was demonstrated in [21] to extend the coverage of VLC. All of the previous studies have focused on PNC's advantages in optical relay systems. In this paper, we make the first attempt to extend PNC to a point-to-point VLC system to deal with the ambient background light interference problem.

The contributions of this paper are as follows:

- 1) We study a VLC system using RGB LEDs transmitting three streams of information in parallel, and focus on the SNR degradation problem due to the saturation of PD caused by ambient light using closed form expressions.
- 2) To mitigate the ambient light interference, we propose PNC-VLC, a network-coded transmission technique that makes use of two LEDs with the same color to transmit two different streams simultaneously, and at the receiver, PNC-VLC can exploit the naturally overlapped optical signal to formulate PNC and finally improve the system BER performance.
- 3) Three International Commission on Illumination (CIE) illuminants and one commercial white LED inference model are used to prove the robustness and stability of the PNC-VLC system over the traditional RGB-VLC system. Simulation results show that, with 2/3 throughput efficiency, PNC-VLC can bring up to 133.3% gain to the BER performance at the FEC limit.

The system structure of PNC-VLC is shown in Fig. 2 and the explanation of symbols inside can be found in section V. At the transmitter, two LEDs with the same color are used to transmit

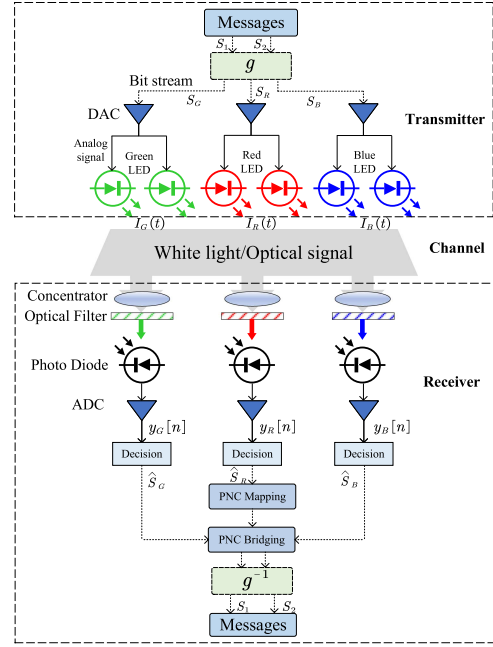


Fig. 2. The proposed PNC-VLC system based on RGB LEDs.

two different packets simultaneously. Two optical signals emitted from the same color LEDs will naturally superimpose at the receiver. An exclusive OR (XOR) message will be obtained from the superimposed signal and then, the PNC decoding procedure will be executed for getting a better result. Compared with the traditional RGB-VLC system shown in Fig. 1, transmitting three data streams independently, the hardware difference is small, and the distinct difference is the digital signal processing. We prove the superiority of the PNC-VLC system under the influence of complex ambient light via simulations. Four kinds of ambient light are applied and the results show that the PNC-VLC system performs better than the traditional RGB-VLC system.

## II. PRELIMINARIES

Among many studies that have been published on this topic [22], [23], a radiation intensity pattern LED follows the Lambertian emitter model, which is denoted as

$$I_{\theta}(\lambda) = \frac{m+1}{2\pi} \cos^m(\theta) I_0(\lambda), \quad (1)$$

where  $I_0(\lambda)$  is a reference intensity with an spectral power distribution (SPD);  $m$  denotes the Lambert index related to the source radiation semi-angle  $m = -\frac{1}{\log_2(\cos \Phi_{1/2})}$ , where  $\Phi_{1/2}$  denotes the transmitter semi-angle at half power. From  $\Phi = \int_{\Omega} I d\omega$ ,  $d\omega = I_{\theta} \sin(\theta) d\theta d\phi$ , and  $2\pi \int_0^{\pi} \frac{m+1}{2\pi} \cos^m(\theta) \sin(\theta) d\theta = 1$ , we get  $I_0 = P_t$  and  $P_t$  is the emitted optical power of a light source [24]. From [25], a linear relationship between emitted optical power and the driving current into the LED can be simply denoted as

$$P_t = \eta_{ext} \eta_{int} \frac{h c i}{e \lambda_d} p(\lambda), \quad (2)$$

where  $h = 6.626 \times 10^{-34}$  Js is Planck's constant;  $e = 1.60217663 \times 10^{-19}$  C is the elementary charge;  $c$  is the velocity of light in the vacuum;  $i$  is the driving current across the device;  $\lambda_d$  is the dominated wavelength in this paper;  $p(\lambda)$  is the normalized PSD;  $\eta_{ext}$  is the external quantum efficiency; and  $\eta_{int}$  is the internal quantum efficiency.

Considering a detector mounted with a concentrator and filter, the effective signal-collection area of the detector is

$$A_r(\phi) = \begin{cases} AT(\lambda)g(\phi)\cos(\phi), & 0 \leq \phi \leq \psi_c \\ 0, & \phi > \psi_c \end{cases}, \quad (3)$$

where  $A$  is the photosensitive area of the detector,  $\Phi$  is the angle of incidence;  $T_\lambda(\phi)$  is the transmission of the filter;  $g(\phi)$  is the concentrator gain, and  $\psi_c$  is the concentrator FOV and usually smaller than  $\frac{\pi}{2}$ . From [22], the maximum concentration ratio for a circular concentrator is

$$g(\varphi) = \begin{cases} \frac{n_1^2}{n_2^2 \sin^2 \psi_c}, & 0 \leq \varphi \leq \psi_c \\ 0, & \varphi > \psi_c \end{cases}, \quad (4)$$

where  $n_1$  and  $n_2$  are the refractive indices of the media in which the entrance and exit apertures are immersed. Because the concentrator and detector are placed in the air, the  $n_1/n_2 = 1$ . The received optical power or radiant flux can be denoted as

$$P_r(\lambda) = \int_{\lambda} \frac{I_\theta(\lambda) A_r(\varphi)}{d^2} d\lambda. \quad (5)$$

In practice, the extra incident ambient light promotes the DC photocurrent and may cause the PD to be saturated. The resulting DC photocurrent brings more shot noise and thermal noise. The ambient light is usually assumed to be isotropic, so the received optical power of the ambient light is given by

$$P_n(\lambda) = \int_{\lambda} E_n(\lambda) A_r(\varphi) d\lambda, \quad (6)$$

where  $E_n(\lambda)$  is the spectral irradiance of the incident ambient light. In summary, the photocurrent generated by a PD is given by

$$i(t) = i_r + i_{sh}(t) + i_{th}(t), \quad (7)$$

where  $i_r = \int_{\lambda} R(\lambda)(P_r(\lambda) + P_n(\lambda))d\lambda$  is the average current only related to the optical power and  $R(\lambda)$  is the responsivity of the detector;  $i_{sh}(t)$  is a current fluctuation due to shot noise, and  $i_{th}(t)$  is a current fluctuation induced by thermal noise. The shot noise and thermal noise are two main noise mechanisms responsible for current fluctuations in silicon-based detector [26]. The  $\sigma_{sh}^2$  of a PIN is given by

$$\sigma_{sh}^2 = 2q \left( \int_{\lambda} R(\lambda) P_{total}(\lambda) d\lambda + i_d \right) \Delta f, \quad (8)$$

where  $q$  is the electron charge;  $i_d$  is the dark current;  $\Delta f$  is the effective noise bandwidth of the receiver, and  $P_{total}$  is the total incident power including optical signal and ambient light. The noise variance  $\sigma_{th}^2$  is given by

$$\sigma_{th}^2 = \frac{4hT\Delta f}{R_L}, \quad (9)$$

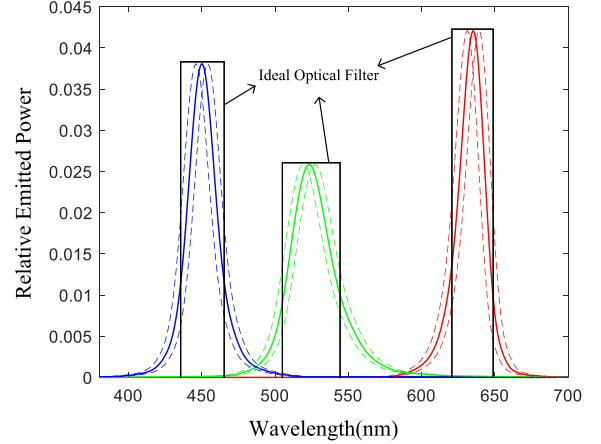


Fig. 3. The PSDs of tri-color LED.

where  $h$  is the Boltzmann constant;  $T$  is the absolute temperature; and  $R_L$  is the load resistor. From (9), the incident optical power does not influence  $\sigma_{th}^2$  unless it could heat the PD. The thermal noise is induced by the random thermal motion of electrons in a resistor, even if no voltage is applied. The SNR of the receiver is given by

$$\text{SNR} = \frac{i_r^2}{\sigma_{th}^2 + \sigma_{sh}^2}. \quad (10)$$

### III. THE COLORIMETRY ISSUE IN VLC

The chroma of hybrid white light generated by tri-color LEDs is critical to users. Usually, adjusting the emitted optical power of red, green, and blue LED to be the same cannot generate white hybrid light. Therefore, it is important to compute the optical power ratio between red, green, and blue light to guarantee available lighting. In colorimetry, the CCT is a familiar character to evaluate the white light [27]. Not all lights have CCT, only those whose chromatic coordinates are nearby the Planckian locus. In other words, only the white light has CCT. If the chromaticity coordinate of the white light deviates too far from the Planck locus, then the white light seems to be green or purple, and it is not suitable for illumination [24]. To compute the chromaticity coordinate and CCT of the white light, we first need its PSD. The PSD of the tricolor LED used is shown in Fig. 3 and is denoted as  $P_{t,R}(\lambda)$ ,  $P_{t,G}(\lambda)$  and  $P_{t,B}(\lambda)$ . The PSD of hybrid light is  $P_t(\lambda) = P_{t,R}(\lambda) + P_{t,G}(\lambda) + P_{t,B}(\lambda)$ . From [27], [28], the tristimulus values of a nonmonochromatic light source are given by

$$X = \int_0^\infty P_t(\lambda) \bar{x}(\lambda) d\lambda, \quad (11)$$

$$Y = \int_0^\infty P_t(\lambda) \bar{y}(\lambda) d\lambda, \quad (12)$$

$$Z = \int_0^\infty P_t(\lambda) \bar{z}(\lambda) d\lambda, \quad (13)$$

where  $\bar{x}(\lambda)$ ,  $\bar{y}(\lambda)$  and  $\bar{z}(\lambda)$  are the spectral color-matching functions of the CIE 1931 2° standard observer. The chromaticity

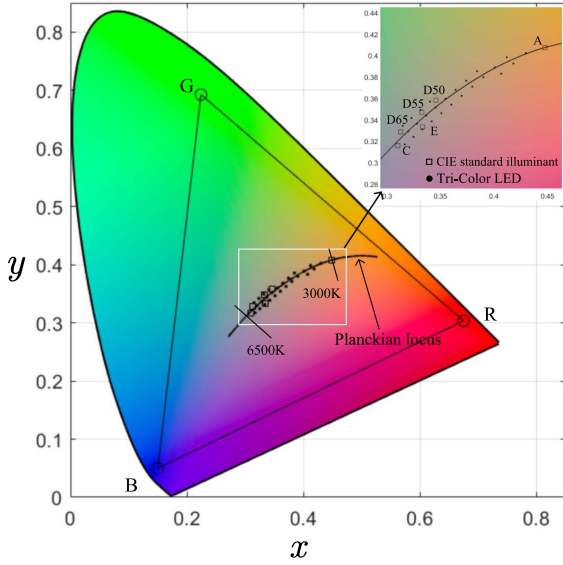


Fig. 4. The 1931 CIE chromaticity diagram and the mentioned CCT coordinates.

coordinates in the 1931 chromaticity diagram can be denoted as

$$x = \frac{X}{X + Y + Z}, \quad (14)$$

$$y = \frac{Y}{X + Y + Z}, \quad (15)$$

$$z = \frac{Z}{X + Y + Z} = 1 - x - y. \quad (16)$$

The color space of the tri-color LED like a triangle in the 1931 chromaticity diagram is shown in Fig. 4. The color space indicates that any colors in the triangle area can be generated from the tri-color LED.

For the demand of the illumination, only the chromaticity coordinates nearby the Planckian locus are considered. The commonly used CCT for lighting is 3000 K to 6500 K. The CCT of hybrid light with equal optical power is about 9850 K and is not suitable for illumination. It is difficult to directly compute the emitted power ratio of the tri-color LED from its PSD and the target CCT. Therefore, we use the exhaustive method to find some chromaticity coordinates in the color space and exclude the points far away from the Planckian locus. It is worth noting that there is no rule to define the boundary of the area nearby the Planckian locus. By adjusting the power ratio of three LEDs, we obtain some different chromaticity coordinates, which are depicted with black dots in Fig. 4. In contrast, we also mark some standard illuminants in Fig. 4, which are denoted as rectangles. We find that it is reasonable to select these coordinates. The minimum CCTs in these available coordinates is 3111 K and the corresponding optical power ratio of red, green, and blue light is 0.68:0.24:0.08. The maximum CCT is 6535 K, with a power ratio of 0.46:0.28:0.26. The average power ratio of the listed coordinates is 0.56:0.26:0.18, which corresponds to 4565 K. We use this setting in all our simulations.

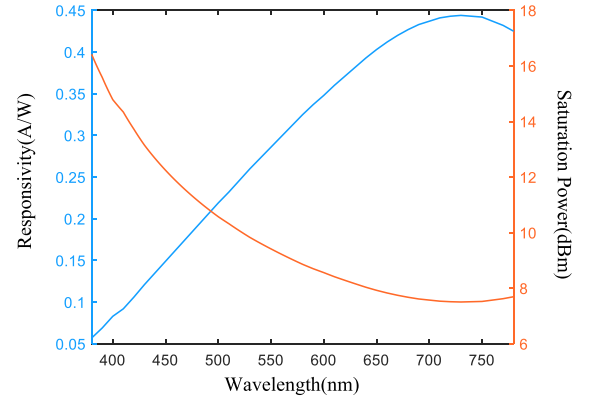


Fig. 5. The responsivity and saturation incident power of PD.

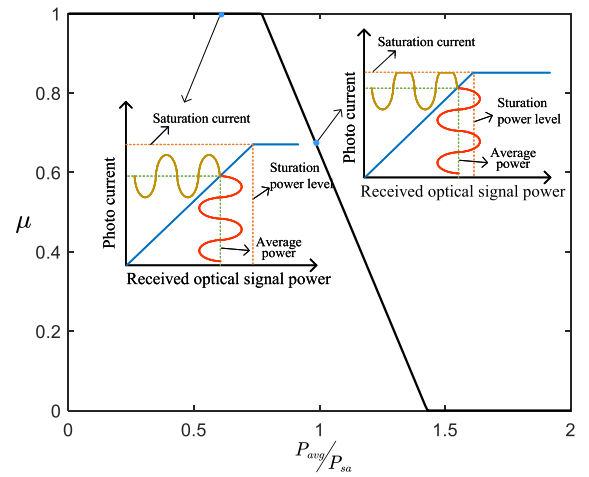


Fig. 6. The clipping coefficient varies with the ratio of  $P_{avg}$  and  $P_{sa}$ .

#### IV. THE SATURATION ISSUE OF A PHOTODIODE

A photodiode (PD) can only linearly convert the incident light into an electrical signal within a limited optical power. The PD will be saturated when the incident optical power goes beyond the detection capability of a PD. Saturation has been attributed primarily to space-charge effects. When it occurs, the responsivity decreases and no additional photocurrent output from the PD as the incident optical power increases [29]. There is also a sharp increase in harmonic distortion [30]. In this paper, we mainly consider the influence caused by saturation on the magnitude of the output AC signal. The saturation power of a photodiode is closely related to the maximum current output and the wavelength-dependent responsivity. The researchers from THORLABS and NEWPORT company study the saturation characteristic and give a simple equation to compute the saturation incident power [31], [32]:

$$P_{sa}(\lambda) = \frac{i_{\max}}{R(\lambda)}, \quad (17)$$

It should be noted that the  $P_{sa}(\lambda)$  only represents the saturation power when the incident light has a single wavelength. From Fig. 6, we know that a PD is more easily saturated to detect the light where the PD is more sensitive to it. When the incident optical

power goes beyond the saturation power level, a clipping occurs on the output AC signal. The additional ambient background radiation equivalently decreases the saturation power level and results in worse clipping. In the worst circumstance, the AC signal may vanish because the minimum instantaneous power of the incident light is still higher than the saturation power. [33] uses the clipping ratio to describe the influence on decreasing amplitude and verifies that the clipping ratio could rise to 80% as the incident ambient light power increases in the experiment. In other words, the ambient light power causes attenuation to the signal power. when the PD works nearby the saturation limit. To simply describe the influence of saturation on the magnitude of the output AC signal, we define a coefficient as follows:

$$\mu = \begin{cases} 1, & P_{avg} \leq \frac{P_{sa}}{1+\beta} \\ -\frac{(1-\beta)(1+\beta)}{2\beta} \frac{P_{avg}}{P_{sa}} + \frac{1+\beta}{2\beta}, & \frac{P_{sa}}{1+\beta} < P_{avg} < \frac{P_{sa}}{1-\beta} \\ 0, & P_{avg} \geq \frac{P_{sa}}{1-\beta} \end{cases}, \quad (18)$$

where  $\beta$  is the modulation depth;  $P_{avg}$  is the average incident optical power, and is decided by incident optical signal and ambient background light. Fig. 6 shows the variation curve of  $\mu$  at  $\beta = 0.3$ . Although a higher modulation depth is of benefit to a bigger AC signal at the receiver, it increases the possibility of clipping on the output signal of PD.

## V. PNC-VLC SYSTEM DESIGN

### A. Working Flow of RGB-VLC and PNC-VLC

In the traditional RGB-VLC system, the message to be transmitted is divided into three streams, which are called  $S_j = (s_j[n])_{n=1, \dots, N}$ ,  $j \in J$  and  $J = \{1, 2, 3\}$ . The modulated optical signal can be denoted as

$$I_k(t) = h_j i_{ac} \sum_{n=0}^{N-1} s_j[n] p(t - nT) + h_j i_{dc}, k \in J, \quad (19)$$

where  $h_j = \eta_{ext} \eta_{int} \frac{hc}{e\lambda_d} p(\lambda)$  from (2) is the emission efficiency;  $i_{ac}$  is the magnitude of AC current;  $T$  is the symbol duration;  $i_{dc}$  is the DC biasing current; and  $p(t)$  is the effective pulse shaping function and the rectangular pulse function is adopted in this paper;  $K = \{R, G, B\}$  is a set that denotes all optical channels.

In the traditional RGB-VLC system, three data streams  $S_j$  are imposed on the LEDs to generate three color optical signals  $I_k(t)$ , respectively. The Data-to-RGB mapping function from  $J$  to  $K$  is denoted as  $f: J \rightarrow K$ . The  $f$  is a bijective function which means it is reversible, representing the one-to-one correspondence between three data streams with three color lights. For example, we can impose  $S_1$  on the red light,  $S_2$  on the green light, and  $S_3$  on the blue light. Every mapping function is a relation from  $M$  to  $L$  or one set of all ordered pairs. The set of all ordered pairs  $(j, k)$  is called cartesian product  $J \times K$  and  $f$  is a subset  $f \subseteq J \times K$ .

In the PNC-VLC system, the message is divided into two streams  $S_1 = (s_1[n])_{n=1, \dots, N}$ ,  $S_2 = (s_2[n])_{n=1, \dots, N}$  and their combination  $S_{(1,2)} = (s_1[n], s_2[n])_{n=1, \dots, N}$ . The data streams  $S_1$  and  $S_2$  are transmitted by LEDs with two different colors, just the same as traditional RGB-VLC. However, the combination

pair  $S_{(1,2)}$  is transmitted by two LEDs with the same color. There is no doubt that the two optical signals with the same color will naturally overlap and cannot be separated once they are emitted. We define a set  $L = \{1, 2, (1, 2)\}$ , let  $g: L \rightarrow K$  denote the mapping function from  $L$  to  $K$ . It is obvious that  $g$  is also bijective and reversible. The superimposed optical signal doing PNC coding is denoted as

$$I_{g(1,2)}(t) = h_{g(1,2)} i_{ac} \sum_{n=0}^{N-1} s_1[n] p(t - nT) + s_2[n] p(t - nT - \Delta t) + h_{g(1,2)} i_{dc}, \quad (20)$$

where  $\Delta t$  is the relative symbol alignment offset. One may note whether or not two red optical signals could overlap with symbol alignment at the receiver, which means that  $\Delta t$  could be neglected. First, the line length on the PCB board between the signal generator and two red LEDs can be designed to be the same without effort. Second, two LEDs are placed closely and could be regarded as one LED, so the transmission delay of two optical signals in free space can be treated as the same. Therefore, two optical signals will superimpose with symbol alignment at the receiver. In other words, the proposed RGB-PNC scheme is a symbol alignment PNC scheme that is easiest to implement [34].

At the receiver, the target optical signal is distinguished from the white light by different optical filters and then converted into an electrical signal by PD. The receiver demodulates the received signal using a matched filter, followed by a threshold decision [35]. As long as the distance between the transmitter and receiver is large relative to the detector size, the received irradiance is approximately constant over the detector surface and all of the signal's energy arrives at the receiver at approximately the same time [36]. Therefore, after matched filtering and sampling at the bit rate, the discrete signal is given by

$$y_{g(1)}[n] = H_{g(1)}(0) s_1[n] + w[n], \quad (21)$$

$$y_{g(2)}[n] = H_{g(2)}(0) s_2[n] + w[n], \quad (22)$$

$$y_{g(1,2)}[n] = \frac{1}{2} H_{g(1,2)}(0) (s_1[n] + s_2[n]) + w[n], \quad (23)$$

where  $H_k(0) = \frac{(m+1) \cos^m(\theta) A \cos(\varphi)}{2\pi d^2} \frac{\eta_{ext} \eta_{int} hc \mu i_{ac}}{\sin^2 \psi_c e\lambda_d} \int_{\lambda} [R(\lambda) T_{\kappa}(\lambda) p_{\kappa}(\lambda)] d\lambda$  is called the DC channel gain of the red, green and blue channel.

In the traditional RGB-VLC system, it is easy to implement the operation to decide if these samples are bit 0 or bit 1. However, the operation is different for the PNC-VLC system. In the following discussion, the recovered stream from  $y_{g(l)}$  is denoted as  $\hat{S}_{g(l)}$ , the recovered streams from PNC decoding (namely, PNC bridging) are denoted as  $\tilde{S}_{g(1)}$  and  $\tilde{S}_{g(2)}$ , respectively. In the channel of implementing PNC coding, the received signal is the superposition of two different signals, so we need to decide and map the samples into the XOR value of the transmitted bits. The PNC-VLC decision and mapping rule is presented in Fig. 8. After recovering  $\hat{S}_{g(1)}$ ,  $\hat{S}_{g(2)}$ , and  $\hat{S}_{g(1,2)}$ , the extra decoding step is implemented:

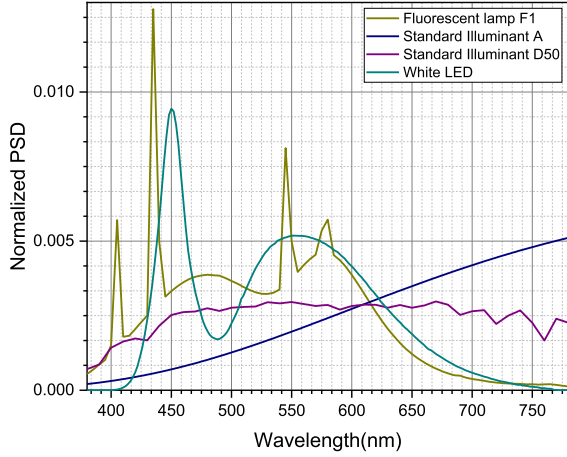


Fig. 7. The PSDs of four ambient lights [37].

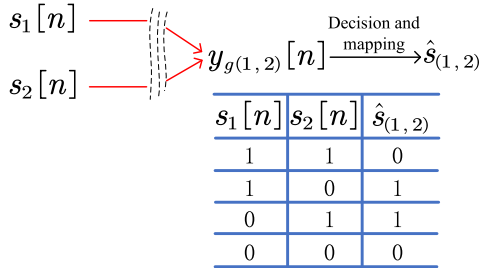


Fig. 8. The PNC decision rule in the PNC-VLC system.

*Step 1:* Use operation  $\hat{S}_{g(1)} \oplus \hat{S}_{g(1,2)}$  to recover  $\tilde{S}_{g(2)}$  and use operation  $\hat{S}_{g(2)} \oplus \hat{S}_{g(1,2)}$  to recover  $\tilde{S}_{g(1)}$ .

*Step 2:* Compare  $\tilde{S}_{g(1)}$  with  $\hat{S}_{g(1)}$  and compare  $\tilde{S}_{g(2)}$  with  $\hat{S}_{g(2)}$ , then choose the best one as the recovered message.

The symbol “ $\oplus$ ” denotes the XOR operation. We list the following example to explain the complete PNC bridging procedure. Assuming that the received signal  $y_{g(2)}$  is bad at a time slot, the recovered  $\hat{S}_{g(2)}(t)$  is an error message. Fortunately, the  $y_{g(1)}$  and  $y_{g(1,2)}$  are better so that  $\hat{S}_{g(1,2)}$  and  $\hat{S}_{g(2)}$  are correct at most time and the recovered  $\tilde{S}_{g(1)}$  is more correct than  $\hat{S}_{g(1)}$ . Therefore, we could choose the best one of  $\tilde{S}_{g(1)}$  and  $\hat{S}_{g(1)}$  through comparing their BER. We can also compare their soft information or use other combination methods like maximum ratio combination(MRC) and so on, this issue will be studied in future works. If the  $y_{g(1)}$  is bad at another time slot, we can use the same decoding procedure to recover  $\tilde{S}_{g(2)}$  without any changes. Although the PNC-VLC system lost the 1/3 channel capacity compared with the RGB-VLC system, it makes the VLC system more robust and stable.

In practice, any one of the three channels in the RGB-VLC system may be heavily affected because of the complex and varied ambient light. A traditional VLC system with three independent links does not prepare for this unexpected circumstance. If one link is interrupted, the receiver must try to inform the transmitter of retransmitting the lost message and adjusting the following transmission strategy such as stopping the bad

TABLE I  
THE BER OF RECOVERED MESSAGE USING XOR OPERATION

$\hat{S}_{g(1)}[n]$	$\hat{S}_{g(1,2)}[n]$	$\tilde{S}_{g(2)}[n]$
right(with1 - $\hat{P}_e^{g(1)}$ )	right(with1 - $\hat{P}_e^{g(1,2)}$ )	right(with1 - $\hat{P}_e^{g(1)}$ )
right(with1 - $\hat{P}_e^{g(1)}$ )	wrong(with $\hat{P}_e^{g(1,2)}$ )	wrong(with $\hat{P}_e^{g(2)}$ )
wrong(with $\hat{P}_e^{g(1)}$ )	right(with1 - $\hat{P}_e^{g(1,2)}$ )	wrong(with $\hat{P}_e^{g(2)}$ )
wrong(with $\hat{P}_e^{g(1)}$ )	wrong(with $\hat{P}_e^{g(1,2)}$ )	right(with1 - $\hat{P}_e^{g(2)}$ )

link. However, frequent feedback and switches in an uncertain environment may heavily decrease communication efficiency. In comparison, the PNC-VLC system does not worry about this problem. It could choose the best two links to reduce the influence of ambient light. More importantly, the adaptivity of the PNC-VLC system could handle the interruption of anyone link without any changes in the transmitter and receiver.

### B. BER Analysis of PNC-VLC

For a more explicit description, we use  $\hat{P}_e^k$  to represent the BER of the recovered message from channel  $k$ . Each  $\hat{P}_e^k$  also equals the BER of the stream  $S_l$  denoted as  $P_e^l$ , following the mapping function  $g$ . Using  $\tilde{P}_e^{g(1)}$  and  $\tilde{P}_e^{g(2)}$  to denote the BER of  $\tilde{S}_{g(1)}$  and  $\tilde{S}_{g(2)}$ , respectively, they are calculated from  $\hat{P}_e^k$ . For example, we aim to calculate  $\tilde{P}_e^{g(2)}$  from  $\hat{P}_e^{g(1)}$  and  $\hat{P}_e^{g(1,2)}$ , then we have the analysis in Table. I.

The BER of  $\tilde{S}_{g(1)}$  is given by

$$\begin{aligned} \tilde{P}_e^{g(2)} &= (1 - \hat{P}_e^{g(1)}) \hat{P}_e^{g(1,2)} + (1 - \hat{P}_e^{g(1,2)}) \hat{P}_e^{g(1)} \\ &= \hat{P}_e^{g(1,2)} + \hat{P}_e^{g(1)} - 2\hat{P}_e^{g(1)}\hat{P}_e^{g(1,2)}, \end{aligned} \quad (24)$$

Similarly, we can get  $\tilde{P}_e^{g(1)}$ :

$$\tilde{P}_e^{g(1)} = \hat{P}_e^{g(1,2)} + \hat{P}_e^{g(2)} - 2\hat{P}_e^{g(2)}\hat{P}_e^{g(1,2)} \quad (25)$$

After executing the last PNC bridging step, we get the final BER:

$$\bar{P}_e^{g(1)} = \min \{ \tilde{P}_e^{g(1)}, \hat{P}_e^{g(1)} \}, \bar{P}_e^{g(2)} = \min \{ \tilde{P}_e^{g(2)}, \hat{P}_e^{g(2)} \}, \quad (26)$$

For a given mapping function  $g$ , we can easily get the final BER of recovered streams  $\hat{S}_1$  and  $\hat{S}_2$ :  $P_e^l = \bar{P}_e^{g^{-1}(g(l))}$ .

At the transmitter, the modulated signal is a DC-biased signal, so that the received signal  $y_k[n] \in A = \{\sqrt{E_H}, \sqrt{E_L}\}$ , that is  $y_k[n] = s_j[n](\sqrt{E_H} - \sqrt{E_L}) + \sqrt{E_L}$ . where  $E_H$  is the energy of bit 1 and  $E_L$  is the energy of bit 0. From [34], the posterior probability of the combination  $(s_1[n], s_2[n])$  is given by

$$\begin{aligned} \Pr(A \times A | y_{g(1,2)}[n]) &= \frac{\Pr(y_{g(1,2)}[n] | A \times A)}{4\Pr(y_{g(1,2)}[n])} \\ &= \frac{1}{4\Pr(y_{g(1,2)}[n])\sqrt{\pi N_0}} \\ &\quad \times \exp \left\{ \frac{|y_{g(1,2)}[n] - y_{g(1)}[n] - y_{g(2)}[n]|}{N_0} \right\}, \end{aligned} \quad (27)$$

where  $N_0 = 2\sigma^2$  is noise power spectral density. For hard decision, let  $\gamma_1 = \frac{3}{2}\sqrt{E_L} + \frac{1}{2}\sqrt{E_H}$  and  $\gamma_2 = \frac{3}{2}\sqrt{E_H} + \frac{1}{2}\sqrt{E_L}$

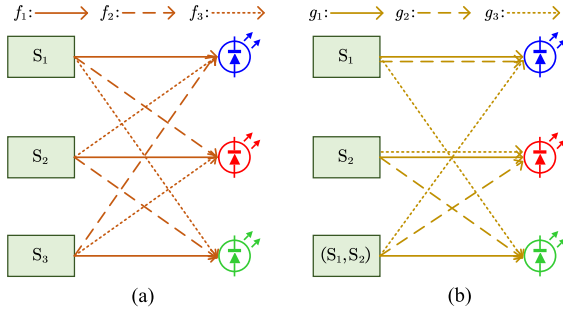


Fig. 9. An example of the connection relations between data streams  $S_l$  with RGB LEDs.

denote the decision thresholds, so the BER can be calculated by (28) shown at the bottom of this page.

For simplicity, the current thresholds are sub-optimal in the low SNR regime, and the optimal thresholds can be found using methods in Chapter 4 of [38]. Let  $\text{SNR} = \frac{E_b}{N_0/2}$ ,  $\sqrt{E_b} = \sqrt{E_H} - \sqrt{E_L}$ , for the biased NRZ-OOK modulation in this paper, we have

$$\text{BER} = \frac{3}{2}Q\left(\frac{\sqrt{\text{SNR}}}{2}\right) - \frac{1}{2}Q\left(\frac{3\sqrt{\text{SNR}}}{2}\right), \quad (29)$$

Compared with the traditional RGB-VLC system in Fig. 1, the  $\sqrt{E_b} = \frac{1}{2}(2\sqrt{E_H} - 2\sqrt{E_L})$ , so the SNR is the same as PNC-VLC and from [38], we know the BER of the channel with doing PNC coding is  $Q(\sqrt{\text{SNR}})$ .

In the above subsection, we briefly discuss the mapping function  $f$  and  $g$ , which represent the connection relationship between source streams and LEDs. In the mapping functions shown in Fig. 9(a) of the traditional RGB-VLC. If we adopt  $f_1$ , then we have  $f_1(1) = R$ ,  $f_1(2) = G$ , and  $f_1(3) = B$ . Due to the difference between R, G, and B channels, the  $f_1$  decides which one of  $\hat{S}_1$ ,  $\hat{S}_2$ , and  $\hat{S}_3$  is the best. Therefore, the mapping function  $f$  could hugely influence the BER of the individual link. We could focus on the system BER which is derived from three BERs of red, green, and blue channels, reflecting the overall performance of the whole VLC system, it can be calculated by

$$P_e^{sys} = \frac{1}{3}(P_e^1 + P_e^2 + P_e^3), \quad (30)$$

Similar to the RGB-VLC, we could also calculate the system BER of PNC-VLC from

$$P_e^{sys} = \frac{1}{2}(P_e^1 + P_e^2). \quad (31)$$

In the RGB-VLC system, the  $f$  doesn't influence the system BER, while in the PNC-VLC system, the circumstances may be different. We divide all functions of  $L \times K$  into 3 cases:

*Case-1:* Use the best channel to do PNC coding. An example is  $g_2$  in Fig. 9(b).

*Case-2:* Use the moderate channel to do PNC coding. An example is  $g_1$  in Fig. 9(b).

*Case-3:* Use the worst channel to do PNC coding. An example is  $g_3$  in Fig. 9(b).

For the convenience of discussion, we assume that the red, green, and blue channels are the best, moderate, and worst, respectively. Their SNRs have a significant difference. In Case-1,  $g(1, 2) = R$ , so  $\hat{P}_e^{g(1,2)} = \hat{P}_e^R$  denotes the BER of recovered XOR message. The connection relations between the green channel with  $S_1$  and the blue channel with  $S_2$  are arbitrary. We could make  $g(1) = G$ , so  $\hat{P}_e^{g(1)} = \hat{P}_e^G$ . The blue channel can be abandoned because it is the worst and the recovered information is useless. From PNC decoding, the BER of  $S_1$  and  $S_2$  are  $P_e^1 = \hat{P}_e^G$  and  $P_e^2 = \hat{P}_e^R + \hat{P}_e^G - 2\hat{P}_e^R\hat{P}_e^G$ , so that the system BER is

$$P_e^{sys} = \frac{1}{2}\hat{P}_e^R + \hat{P}_e^G - \hat{P}_e^R\hat{P}_e^G, \quad (32)$$

In Case-2),  $P_e^1 = \hat{P}_e^R$ ,  $P_e^2 = \hat{P}_e^R + \hat{P}_e^G - 2\hat{P}_e^R\hat{P}_e^G$ , so that the system BER is

$$P_e^{sys} = \hat{P}_e^R + \frac{1}{2}\hat{P}_e^G - \hat{P}_e^R\hat{P}_e^G, \quad (33)$$

In Case-3), the recovered PNC XOR message that comes from the blue channel has the worst performance so it is abandoned. The  $S_1$  and  $S_2$  are directly recovered from  $\hat{S}_R$  and  $\hat{S}_G$ , so the system BER is

$$P_e^{sys} = \frac{1}{2}(\hat{P}_e^R + \hat{P}_e^G). \quad (34)$$

From the above discussion, we know the system BER of PNC-VLC is only decided by the two best channels. The  $g$  could slightly influence the system BER, with respect to Fig. 11, the difference of system BERs in three cases is no more than 1.4%. The characteristic brings an advantage to the PNC-VLC system, that is the performance could keep stable in different ambient lights without changing the mapping function  $g$ .

## VI. SIMULATION RESULTS AND DISCUSSION

In our simulation, only LOS channel gain is considered. For simplicity, some simulation parameters are acquired from the COTS devices. The simulation setup is shown in Table. II. The

$$\text{BER} = \frac{1}{2} \left[ Q\left(\frac{\gamma_2 - (\sqrt{E_H} + \sqrt{E_L})}{\sqrt{\frac{N_0}{2}}}\right) + Q\left(\frac{-\gamma_1 + (\sqrt{E_H} + \sqrt{E_L})}{\sqrt{\frac{N_0}{2}}}\right) \right] + \frac{1}{4} \left[ Q\left(\frac{\gamma_1 - 2\sqrt{E_H}}{\sqrt{\frac{N_0}{2}}}\right) + Q\left(\frac{\gamma_1 - 2\sqrt{E_L}}{\sqrt{\frac{N_0}{2}}}\right) \right] - \frac{1}{4} \left[ Q\left(\frac{\gamma_2 - 2\sqrt{E_H}}{\sqrt{\frac{N_0}{2}}}\right) + Q\left(\frac{\gamma_2 - 2\sqrt{E_L}}{\sqrt{\frac{N_0}{2}}}\right) \right], \quad (28)$$

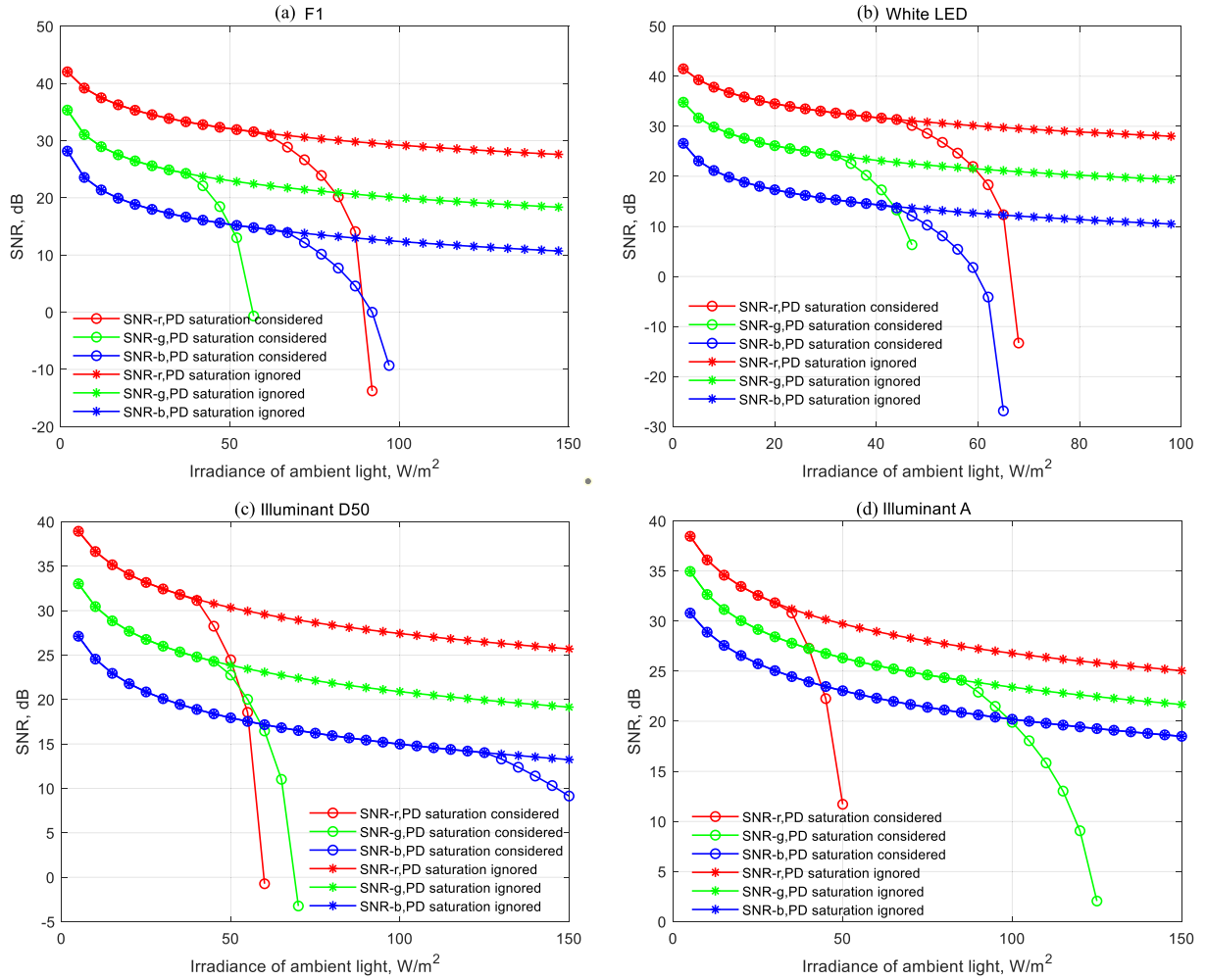


Fig. 10. The SNRs of the red, green, and blue channels (called SNR-r, SNR-g, and SNR-b, respectively) under the influences of four different ambient lights: (a) Fluorescent lamp F1, (b) Endura OT16-3101-WTMR16 white LED, (c) Standard Illuminant D50, (d) Standard Illuminant A.

TABLE II  
THE SIMULATION SETUP

<b>Transmitter</b>	LED	OSRAM LE RTB N7WM
	Semi-angle	80deg
	Total Emitting Power	10W
	Transmission Distance	3m
<b>Concentrator</b>	Focal Length	25mm
	Diameter	25.4mm
<b>Receiver</b>	PIN	Thorlabs DET10A2
	Active Area Diameter	1mm
<b>Ambient Light</b>	Irradiance	1-200W/m <sup>2</sup>

PSD data of the tri-color LED is drawn from the OSRAM LE RTB N7WM datasheet. The semi-angle is set as 80 degrees and the transmission distance is 3 m. The parameters of the PIN receiver come from Thorlabs DET10A2. Four typical ambient light sources with the same emission power are shown in Fig. 7: Fluorescent lamp F1, CIE Standard Illuminant A, D50, and Endura OT16-3101-WTMR16 LED are used to produce the ambient light in the simulation.

The power ratio of red, green, and blue light is set as 0.56:0.26:0.18. The PSD of the tri-color LED is shown in Fig. 3. The red, green, and blue solid lines are typical PSD curves of the

tri-color LED and the surrounding two dashed lines near the solid line represent the maximum offset of the dominant wavelength among different LEDs. Three black rectangles represent the ideal optical filter, their maximum transmissions are assumed to be 1 and the full-width half maximum (FWHM) is decided by the PSD of tri-color LED and dominant wavelength offset. However, the transmission curve of a practical optical filter is surely not like that. This question will be studied in future work. In the receiver, different ambient lights impose variable influences on their PD. Although the optical filter could isolate most of the energy of the incident ambient light, it could not isolate the light within the transmission scale of the optical filter.

In our simulation, we no longer treat the ambient light source as a Lambertian emitter because we do not care about the emission characteristic of the illuminant. Fig. 10 shows that the SNR varies with the irradiance of ambient light. The three solid lines with asterisk symbols represent the SNR without the influence of saturation power limit and the ambient light only brings more shot noise. The decreasing rate of the SNR curves becomes smaller as the irradiance increases. When only considering the shot noise the ambient light brings, it is not enough to reflect its influences in the VLC system. In practice,



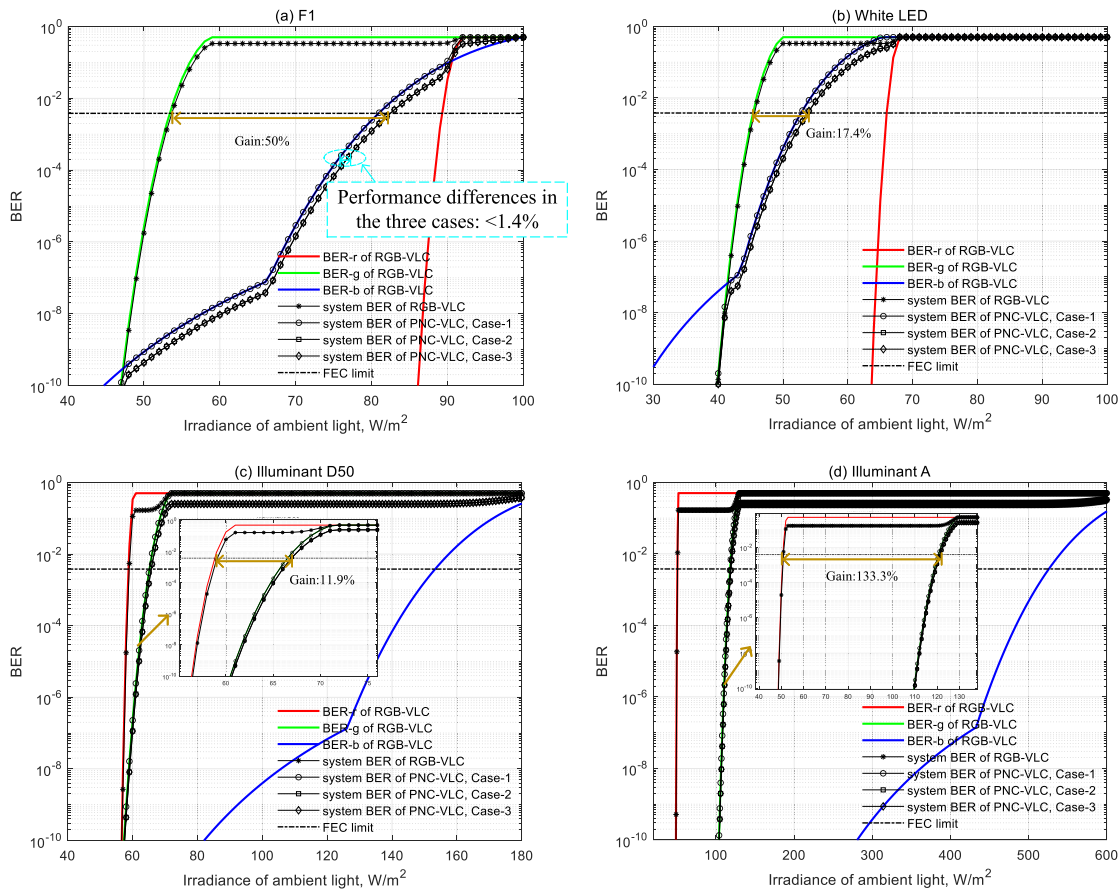


Fig. 11. The BER performance of the RGB-VLC and PNC-VLC systems under four different ambient light conditions: (a) Fluorescent lamp F1, (b) Endura OT16-3101-WTMR16 white LED, (c) Standard Illuminant D50, (d) Standard Illuminant A. The BERs of three channels are called BER-r, BER-g, and BER-b, respectively. The gain is calculated at the FEC limit  $3.8 \times 10^{-3}$ .

the problems caused by saturation cannot be neglected. The power sum of the collected optical signal and ambient light may exceed the linear conversion region of a PD and higher incident power may permanently damage the PD. The three solid lines with circle symbols show the simulation results using the saturation mode in Section IV. We can see that a change happens on the SNR curve once the PD enters the saturation region. When the incident power increases continuously, the SNR performance degrades rapidly and three VLC links are interrupted with different orders. When the ambient light is Fluorescent lamp F1, the PD of the green link will reach the saturation limit first. However, in Standard Illuminant A, the PD of the red link reaches the saturation limit earlier than the other two PDs. In Standard Illuminant D50, the red and green links almost reach the saturation limit simultaneously. Under the influence of Illuminant A and Illuminant D50, the blue link shows better stability, although it has the lowest SNR in the traditional VLC system. The RGB-VLC and PNC-VLC system has the worst performance under the influence of white LED because the PSD is similar to a tri-color LED. As we discussed earlier, the different ambient lights bring different performance degradations to three VLC links. When one of the three links is interrupted, the receiver must inform the transmitter of stopping transmission and retransmitting the message from another link. Therefore, there is no doubt that the feedback

improves the complexity of the VLC system, not to mention that no one can guarantee that the feedback link is reliable. The RGB-PNC scheme could effectively decrease the feedback probability. The most distinct advantage is that the receiver can recover the messages no matter which link is interrupted. The hardware difference between RGB-VLC and PNC-VLC systems is small, only the transmitter of the red link needs modification. The received optical signal power of the PNC-VLC system is the same as the RGB-VLC system, so the SNR performance is also the same as the RGB-VLC system.

Fig. 11 shows the BER performance of RGB-VLC and PNC-VLC systems. The system BER of the two VLC systems could reflect the performance difference more directly. In the RGB-VLC system, the system BER is mainly influenced by the worst link. However, in PNC-VLC, the redundant information could lower the error probability of recovering the message. Therefore, the system BER of the PNC-VLC is decided by the two best links. The advantage of PNC-VLC is fully demonstrated when the ambient light source is Illuminant A, which brings 133.3% gain at the FEC limit. In this case, although the emitted optical power of the red LED is the biggest, the red link has the lowest SNR and worst BER. Besides, the system BER of the RGB-VLC system is almost as same as the red link, even though the green and blue links have better performance. In contrast, in the PNC-VLC, the receiver could recover the messages from

the green and blue links. So the system BER of the PNC-VLC system is almost the same as the green link and is far better than RGB-VLC. In four ambient lights, the gain of PNC-VLC is different. Only 11.9% gain is brought by PNC-VLC under the influence of illuminant D50 due to the huge SNR degradation of the red and green link.

## VII. CONCLUSION

This paper studied two VLC systems affected by different ambient background lights. Conventional RGB-LED based VLC systems transmit three separate data streams in parallel. To overcome the BER degradation problem caused by the ambient light interference in point-to-point RGB-VLC systems, PNC-VLC, a network-coded transmission system was proposed to make use of two same color LEDs at the transmitter to transmit the two different streams and to make use of the naturally overlapped signals detected at the receiver to formulate physical-layer network coding. We find that PNC-VLC can effectively mitigate the BER degradation caused by ambient light using rigorous derivations. We conducted simulations based on commercial off-the-shelf (COTS) products' datasheets, and we use three International Commission on Illumination (CIE) ambient light and one commercial white LED light inference model to prove the superiority of the PNC-VLC. Simulation results proved that the PNC-VLC system can always maintain a stable link under all four illuminants and have better BERs performance than traditional RGB-VLC. The background light interference tolerance gain can be as large as 133.3% in the Illuminant A interference model, with 2/3 throughput efficiency. The main disadvantages of the PNC-VLC system are it uses double LEDs than the traditional RGB-VLC system and a more complex signal processing is needed at the receiver. Going forward, we would like to conduct experiments to further show the robustness of PNC-VLC in real VLC communication scenarios.

## REFERENCES

- [1] P. H. Pathak, X. Feng, P. Hu, and P. Mohapatra, "Visible light communication, networking, and sensing: A survey, potential and challenges," *IEEE Commun. Surveys Tuts.*, vol. 17, no. 4, pp. 2047–2077, Oct.–Dec. 2015.
- [2] M. Popadić and E. Kočan, "LiFi networks: Concept, standardization activities and perspectives," in *Proc. IEEE 25th Int. Conf. Inf. Technol.*, 2021, pp. 1–4.
- [3] X. Wu, M. D. Soltani, L. Zhou, M. Safari, and H. Haas, "Hybrid LiFi and WiFi networks: A survey," *IEEE Commun. Surveys Tuts.*, vol. 23, no. 2, pp. 1398–1420, Apr.–Jun. 2021.
- [4] A. Zubow et al., "Hybrid-fidelity: Utilizing IEEE 802.11 MIMO for practical aggregation of LiFi and WiFi," *IEEE Trans. Mobile Comput.*, 2022, doi: [10.1109/TMC.2022.3157452](https://doi.org/10.1109/TMC.2022.3157452).
- [5] C. Shen et al., "High-speed visible laser light communication: Devices, systems and applications," *Proc. SPIE*, vol. 11711, 2021, Art. no. 1171109.
- [6] P. Qiu et al., "4.0 Gbps visible light communication in a foggy environment based on a blue laser diode," *Opt. Exp.*, vol. 29, no. 9, pp. 14163–14173, 2021.
- [7] C. Lee et al., "26 Gbit/s LiFi system with laser-based white light transmitter," *J. Lightw. Technol.*, vol. 40, no. 5, pp. 1432–1439, Mar. 2021.
- [8] Y. Wang, L. Tao, X. Huang, J. Shi, and N. Chi, "8 Gbit/s RGBY LED-based WDM VLC system employing high-order CAP modulation and hybrid post equalizer," *IEEE Photon. J.*, vol. 7, no. 6, pp. 1–7, Dec. 2015, Art. no. 7904507.
- [9] G. P. Agrawal, *Fiber-Optic Communication Systems*. Hoboken, NJ, USA: Wiley, 2012.
- [10] F. Xu, M.-A. Khalighi, and S. Bourennane, "Impact of different noise sources on the performance of PIN-and APD-based FSO receivers," in *Proc. IEEE 11th Int. Conf. Telecommun.*, 2011, pp. 211–218.
- [11] M. S. Islam et al., "The impact of solar irradiance on visible light communications," *J. Lightw. Technol.*, vol. 36, no. 12, pp. 2376–2386, Jun. 2018.
- [12] S. M. Mana, P. Hellwig, J. Hilt, P. W. Berenguer, and V. Jungnickel, "Experiments in non-line-of-sight Li-Fi channels," in *Proc. IEEE Glob. LIFI Congr.*, 2019, pp. 1–6.
- [13] S. Zhang, S. C. Liew, and P. P. Lam, "Hot topic: Physical-layer network coding," in *Proc. 12th Annu. Int. Conf. Mobile Comput. Netw.*, 2006, pp. 358–365.
- [14] S. C. Liew, L. Lu, and S. Zhang, *A Primer on Physical-Layer Network Coding* (Synthesis Lectures on Communication Networks Series). San Rafael, CA, USA: Morgan & Claypool, 2015.
- [15] S. C. Liew, S. Zhang, and L. Lu, "Physical-layer network coding: Tutorial, survey, and beyond," *Phys. Commun.*, vol. 6, pp. 4–42, 2013.
- [16] Z. Liu, M. Li, L. Lu, C.-K. Chan, S.-C. Liew, and L.-K. Chen, "Optical physical-layer network coding," *IEEE Photon. Technol. Lett.*, vol. 24, no. 16, pp. 1424–1427, Aug. 2012.
- [17] Q. Wang, K.-H. Tse, L.-K. Chen, and S.-C. Liew, "Physical-layer network coding for VPN in TDM-PON," *IEEE Photon. Technol. Lett.*, vol. 24, no. 23, pp. 2166–2168, Dec. 2012.
- [18] Z. Liu, L. Lu, L. You, C.-K. Chan, and S.-C. Liew, "Optical physical-layer network coding over fiber-wireless," in *Proc. IEEE 39th Eur. Conf. Exhib. Opt. Commun.*, 2013, pp. 1–4.
- [19] R. Lin et al., "Physical-layer network coding for passive optical interconnect in datacenter networks," *Opt. Exp.*, vol. 25, no. 15, pp. 17788–17797, 2017.
- [20] R. Lin et al., "First experimental demonstration of physical-layer network coding in PAM4 system for passive optical interconnects," in *Proc. IEEE Eur. Conf. Opt. Commun.*, 2017, pp. 1–3.
- [21] X. Guan, Q. Yang, T. Wang, and C. C.-K. Chan, "Phase-aligned physical-layer network coding in visible light communications," *IEEE Photon. J.*, vol. 11, no. 2, pp. 1–9, Apr. 2019.
- [22] J. M. Kahn and J. R. Barry, "Wireless infrared communications," *Proc. IEEE*, vol. 85, no. 2, pp. 265–298, 1997.
- [23] S. Arnon, *Visible Light Communication*. Cambridge, U.K.: Cambridge Univ. Press, 2015.
- [24] W. R. McCluney, *Introduction to Radiometry and Photometry*. Norwood, MA, USA: Artech House, 2014.
- [25] J. M. Senior and M. Y. Jamro, *Optical Fiber Communications: Principles and Practice*. Upper Saddle River, NJ, USA: Pearson Educ., 2009.
- [26] M. J. Deen and P. K. Basu, *Silicon Photonics: Fundamentals and Devices*. Hoboken, NJ, USA: Wiley, 2012.
- [27] D. Malacara, *Color Vision and Colorimetry: Theory and Applications*. Bellingham, WA: SPIE, 2003.
- [28] R. S. Berns, *Billmeyer and Saltzman's Principles of Color Technology*. Hoboken, NJ, USA: Wiley, 2019.
- [29] P.-L. Liu, K. J. Williams, M. Y. Frankel, and R. D. Esman, "Saturation characteristics of fast photodetectors," *IEEE Trans. Microw. Theory Techn.*, vol. 47, no. 7, pp. 1297–1303, Jul. 1999.
- [30] Y.-L. Huang, "Nonlinear saturation behaviors of high-speed p-i-n photodetectors," *J. Lightw. Technol.*, vol. 18, no. 2, pp. 203–212, 2000.
- [31] "Maximum measurable power for photodiode detector." [Online]. Available: [https://www.photonics.com/White\\_Papers/Maximum\\_Measurable\\_Power\\_for\\_Phodiode\\_Detector/wpp1898](https://www.photonics.com/White_Papers/Maximum_Measurable_Power_for_Phodiode_Detector/wpp1898)
- [32] "Photodiode saturation and noise floor." [Online]. Available: [https://www.thorlabs.com/images/TabImages/Photodetector\\_Lab.pdf](https://www.thorlabs.com/images/TabImages/Photodetector_Lab.pdf)
- [33] W. Liu, Z. Xu, and X. Jin, "Saturation compensation for visible light communication with off-the-shelf detectors," *Opt. Exp.*, vol. 29, no. 6, pp. 9670–9684, 2021.
- [34] L. Lu and S. C. Liew, "Asynchronous physical-layer network coding," *IEEE Trans. Wireless Commun.*, vol. 11, no. 2, pp. 819–831, Feb. 2012.
- [35] Y. Chen, C. W. Sung, S.-W. Ho, and W. S. Wong, "BER analysis for interfering visible light communication systems," in *Proc. IEEE 10th Int. Symp. Commun. Syst., Netw. Digit. Signal Process.*, 2016, pp. 1–6.
- [36] J. R. Barry, J. M. Kahn, W. J. Krause, E. A. Lee, and D. G. Messerschmitt, "Simulation of multipath impulse response for indoor wireless optical channels," *IEEE J. Sel. Areas Commun.*, vol. 11, no. 3, pp. 367–379, Apr. 1993.
- [37] ISO/CIE DIS 11664-2: 2020 (E). Colorimetry. Part 2: CIE Standard Illuminants, 2020.
- [38] E. A. Lee and D. G. Messerschmitt, *Digital Communication*. Berlin, Germany: Springer, 2012.